catalysts

MDPI

Article

Structure and Microchannel Catalytic Bed Performance of Silver Thin Films Prepared by Electroplating

Yong Yang [1,2,3], Yinghua Ye [1,2,3] and Ruiqi Shen [1,2,3,*]

[1] School of Chemistry and Chemical Engineering, Nanjing University of Science and Technology, Nanjing 210094, China; yangyong9998@njust.edu.cn (Y.Y.); yyinghua@mail.njust.edu.cn (Y.Y.)
[2] Micro-Nano Energetic Devices Key Laboratory of MIIT, Nanjing 210094, China
[3] Institute of Space Propulsion, Nanjing University of Science and Technology, Nanjing 210094, China
* Correspondence: rqshen@njust.edu.cn

Abstract: The morphology of catalysts in microchannels plays a crucial role in the orbital maneuvering and networking applications of micro/nano satellites using hydrogen peroxide as a unit propellant. In this paper, a microfluidic reaction chip was designed and fabricated to detect the reaction rate of the catalytic decomposition of hydrogen peroxide solution by a microchannel catalytic bed. In addition, a silver thin film prepared by constant-current electroplating was used as a substrate for the microchannel catalyst. The results show that the ratio of surface area to area of silver film and the average particle size of silver particles have a significant positive correlation on the reaction rate of catalytic decomposition, while the thickness, silver content, and surface roughness of the silver film have no significant effect on the reaction rate of catalytic decomposition. The catalytic performance of the microchannel catalytic bed of silver thin film is greatly influenced by the conditions of electroplating, namely, the electroplating temperature (T), time (t), and current (I). And when I = 0.3 mA, t = 180 s, and T = 60 °C, the microchannel catalytic bed of the silver film prepared by electroplating reaches the optimal reaction rate for the catalytic decomposition of hydrogen peroxide solution. This study has the best process parameters for the design and optimization of heterogeneous catalysts applied to microfluidic reactors.

Keywords: microchannel; catalytic bed; silver; films; electroplating; hydrogen peroxide; microfluidic chips

check for updates

Citation: Yang, Y.; Ye, Y.; Shen, R. Structure and Microchannel Catalytic Bed Performance of Silver Thin Films Prepared by Electroplating. *Catalysts* **2024**, *14*, 39. https://doi.org/10.3390/catal14010039

Academic Editors: Nicolas Abatzoglou and Hugo de Lasa

Received: 10 November 2023
Revised: 28 December 2023
Accepted: 30 December 2023
Published: 5 January 2024

Copyright: © 2024 by the authors. Licensee MDPI, Basel, Switzerland. This article is an open access article distributed under the terms and conditions of the Creative Commons Attribution (CC BY) license (https://creativecommons.org/licenses/by/4.0/).

1. Introduction

Hydrogen peroxide (H_2O_2) is a versatile chemical reagent with a variety of uses, including in disinfectants, antiseptics, bleaches, and oxidants. In high concentrations, it can also be used as a rocket propellant. In rocket propulsion systems, hydrogen peroxide can be used as either a unitary or binary propellant. When used as a unit propellant, [1–4] high-concentration hydrogen peroxide (usually around 70~90%) decomposes into water and oxygen when passing through a decomposition chamber containing a catalyst bed [5]. This process is an exothermic reaction that produces a hot gas that is ejected after acceleration through the rocket nozzle, resulting in thrust [6]. As a binary propellant, hydrogen peroxide is combined with another fuel, such as kerosene or hydrazine, in a binary propellant rocket engine [7]. Hydrogen peroxide acts as an oxidizer, and the other fuel acts as a combustible material [8,9]. When the two propellants are combined and ignited in the combustion chamber, they react chemically to produce hot gases that are expelled through the rocket's nozzle, creating thrust. Hydrogen peroxide propulsion systems have been widely used in the past [10,11], but compared with other propellant combinations such as liquid hydrogen and liquid oxygen in dual-element propulsion systems, the specific impulse and efficiency of hydrogen peroxide propulsion systems are relatively low and are thus less common in modern aerospace. However, hydrogen peroxide is still widely used in some basic fields and experimental projects [6].

Catalysts play a vital role in hydrogen peroxide as unit propellants and binary propellants [12]. They accelerate the decomposition of hydrogen peroxide, and the rate of hydrogen peroxide decomposition is critical to the amount of thrust. For unit propellants, a catalyst promotes the decomposition of hydrogen peroxide into hot gas, producing thrust [13]. In binary propellants, catalysts help control the reaction between hydrogen peroxide and fuel, enhancing combustion and providing better performance. This makes catalysts critical for efficient and reliable propulsion systems in a variety of aerospace applications.

In addition, the use of catalysts in hydrogen peroxide thrusters has several advantages. First, the catalyst achieves a higher energy output by promoting the faster and controlled decomposition of hydrogen peroxide. Another major advantage of catalysts in hydrogen peroxide propulsion systems is their ability to improve safety. At the same time, with the help of catalysts, hydrogen peroxide propellants can initiate catalytic decomposition reactions when needed to provide on-demand thrust, simplifying storage and handling procedures [14]. In addition, the use of catalysts reduces the complexity of propulsion systems in which hydrogen peroxide is used as a unit or dual propellant [15]. Some conventional propellants require a separate ignition system or combustion chamber, but the use of catalysts can simplify the design and reduce the overall weight of the system.

Advanced catalysts can increase the decomposition rate of hydrogen peroxide propellants for better performance. In addition, innovative propulsion concepts, such as combining advanced catalysts, hydrogen peroxide, and other propellants, or optimizing engine design can further improve its overall efficiency and specific impulse [16]. This ongoing work is essential to advance space propulsion technology and enable more efficient and sustainable space missions. There are several types of catalysts that catalyze the decomposition of hydrogen peroxide. Some common types include:

Metal catalysts: these are usually based on transition metals such as platinum, palladium, silver, or gold [17]; metal oxide catalysts: these include catalysts such as manganese oxide, iron oxide, and copper oxide [18]; metal–organic frameworks (MOFs): MOFs are porous materials with high surface areas, and due to their adjustable structure, they are considered catalysts for hydrogen peroxide decomposition [19]; supported catalysts: these catalysts are loaded on a support material, such as alumina or carbon [20,21], to improve its activity and stability [22–24]; and enzymes: some enzymes, such as catalase and peroxidase, can also catalyze the decomposition of hydrogen peroxide [25,26].

As research and development continues, the introduction of novel catalysts could make it possible for hydrogen peroxide-based propulsion systems to play an important role in future space exploration, providing sustainable and adaptive solutions for space missions [3,27].

The application of silver as a hydrogen peroxide catalyst is promising, and ongoing research is aimed at further optimizing its performance, stability, and cost-effectiveness in various fields to make it a valuable component of catalysis and related technologies. The preparation of silver thin films by cyanide-free plating has been of interest due to the environmental and safety concerns associated with the conventional cyanide plating process [28,29]. The use of cyanide in electroplating poses a significant risk to human health and the environment, so it is essential to develop alternative methods. Researchers and the industry have been exploring various cyanide-free plating techniques to deposit silver films. These include: ① non-cyanide silver plating solutions: these solutions use a complexing agent instead of cyanide as a stabilizer for silver ions during the plating process [30,31]; ② chemical deposition: in this method, silver films can be deposited without an external power source because the reduction of silver ions is carried out by a chemical reaction with a reducing agent [32,33]; and ③ electrochemical deposition using non-toxic additives: certain non-toxic additives can enhance the electrochemical deposition of silver without the use of cyanide-based solutions [34]. Significant progress is being made in the development of silver thin film cyanide-free plating technology, and the adoption of this environmentally friendly process is in line with the global shift toward sustainable practices in a variety

of industries, including electronics, coatings, and sensors. The widespread use of silver thin films prepared through these techniques is expected to grow further as technology advances and more efficient non-cyanide plating methods are developed.

Microfluidics has several applications in chemistry due to their ability to handle small amounts of fluids. Microfluidics improve the precision, speed, and efficiency of various chemical processes, making it an important tool for modern chemical research and applications. Microfluidic platforms can be used for miniaturized and sensitive chemical analyses [35] such as DNA sequencing, proteomics, and metabolomics, using reduced sample sizes. The application of microfluidic technology to micro/nano satellite propulsion systems [36] is also a very good choice.

Microreactors for catalysis, also known as microreactor technology or microreactors, are miniaturized devices designed to perform catalytic reactions with enhanced control, efficiency, and safety [37–39]. These microreactors have become increasingly popular in recent years due to their many advantages over conventional batch reactors. These microreactors are characterized by small reaction volumes, strong mass and heat transfer, precise control of reaction parameters, and safer operation. Therefore, they can be widely used in the fields of fine chemical synthesis, green chemistry, continuous flow processing, and high-throughput screening. At the same time, this reactor can also be used for the study and optimization of multiphase and homogeneous catalysts, with advantages in catalyst loading, reaction kinetics, and executive selectivity [40]. Overall, microreactors for catalysis have proven to be powerful tools in chemical research and industrial applications, offering benefits in terms of efficiency, safety, and scalability. The continuous development and integration of catalytic microreactors holds significant promise for the advancement of chemistry [41,42]. Their ability to enable efficient, safe, and sustainable chemical transformations makes them key tools for driving catalytic innovation and addressing societal challenges in chemical synthesis and manufacturing.

The importance of hydrogen peroxide catalysts as unit propellants and dual propellants cannot be neglected. Their ability to achieve efficient and safe propulsion makes hydrogen peroxide an attractive option for a variety of aerospace missions. The selection of a cheap and green hydrogen peroxide catalyst manufacturing method and a microfluidic catalytic performance analysis method are issues that many researchers need to pay attention to. In this study, a silver thin film was electroplated on a nickel sheet by cyanide-free electroplating, and then the microstructure parameters of the silver film were detected using SEM, EDS, and confocal microscopy. The concentration of hydrogen peroxide solution before and after the reaction was determined using ultraviolet-visible spectroscopy in the micro-measuring cell so as to obtain the reaction rate of hydrogen peroxide decomposition under the catalysis of different silver thin films. These parameters are compared to obtain the influence of electroplating conditions on the formation of silver thin films and the variation of the constant of the reaction rate of hydrogen peroxide decomposition.

2. Results and Analysis

2.1. Regression Analysis of SEM Results on Silver Films

Figure 1 shows FESEM micrographs of silver thin films deposited by the electroplating of 16 experimental groups. In addition, the average particle size of the particles on the surface of the silver film was determined using a dimensional measurement tool.

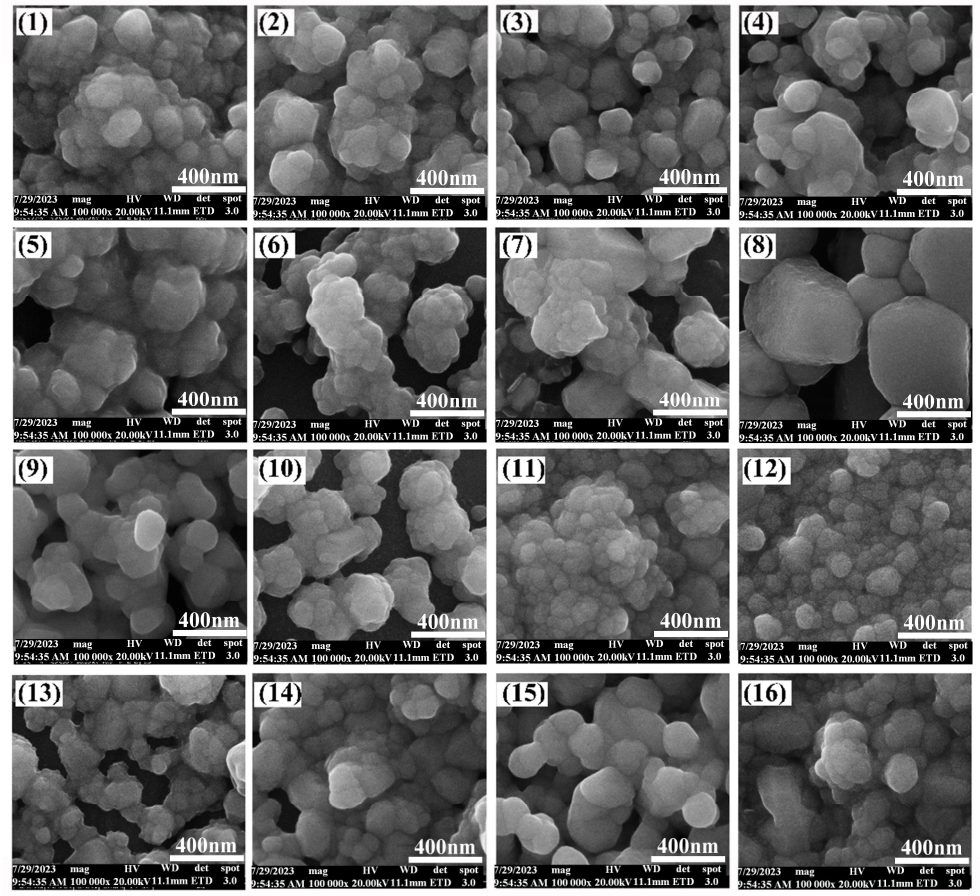


Figure 1. FESEM micrographs of silver thin films deposited by the electroplating of 16 experimental groups.

The method of quadratic orthogonal regression analysis was applied to the regression analysis of the average particle size of particles on the surface of silver film. The results of a regression analysis can be fitted to obtain the quadratic orthogonal regression equation for the average particle size (d) of silver particles, as shown in Equation (1).

$$d = 127.125 + 2.162X_1 - 9.319X_2 - 12.051X_3 + 3.75X_1X_2 + 16X_1X_3 + 39.5X_2X_3 + 11.630X_1\prime - 9.802X_2\prime - 5.576X_3\prime \quad (1)$$

The p-value for this model is 0.027, so this model is significant. The p-value of lack of fit is 0.073, so there is no lack of fit factor. Variance analysis shows that X_3, X_1X_3 have a significant impact on the regression equation ($p_3 = 0.047$, $p_{13} = 0.039$), and X_2X_3 has an extremely significant impact on the regression equation ($p_{23} = 0.001$). According to the magnitude of the coefficients, it can be concluded that the order of influence of these three factors on the average particle size of silver particles on the surface of the film is as follows: plating temperature > plating current > plating time.

Substituting the quadratic term centering formula and coding formula into the above formula, the quadratic regression constraint equation (regression formula) of the average particle size (d) of thin film silver particles can be obtained as

$$d = 947.95 - 2184.24I - 4.772t - 10.616T + 1.031It + 26.40IT + 0.109tT + 1920.40I^2 - 0.0045t^2 - 0.093T^2 \quad (2)$$

We used the Excel solver function to predict the optimal value of the regression Equation (2) under the designed experimental conditions. The results show that the average particle size of the surface particles of the silver film reaches a maximum value of 246 nm and a minimum value of 28 nm.

2.2. Regression Analysis of Silver Content on the Surface of Silver Films

The EDS microscopic results of the silver thin films prepared by electroplating are shown in Figure 2. And taking the silver content as the index, the quadratic orthogonal regression analysis of the silver content on the surface of the silver film can be obtained using a regression analysis, as shown in Equation (3).

$$n = 0.4653 + 0.138X_1 + 0.0516X_2 - 0.0126X_3 + 0.0192X_1X_2 - 0.00492X_1X_3 + 0.0214X_2X_3 - 0.0849X_1' + 0.00413X_2' - 0.0826X_3' \quad (3)$$

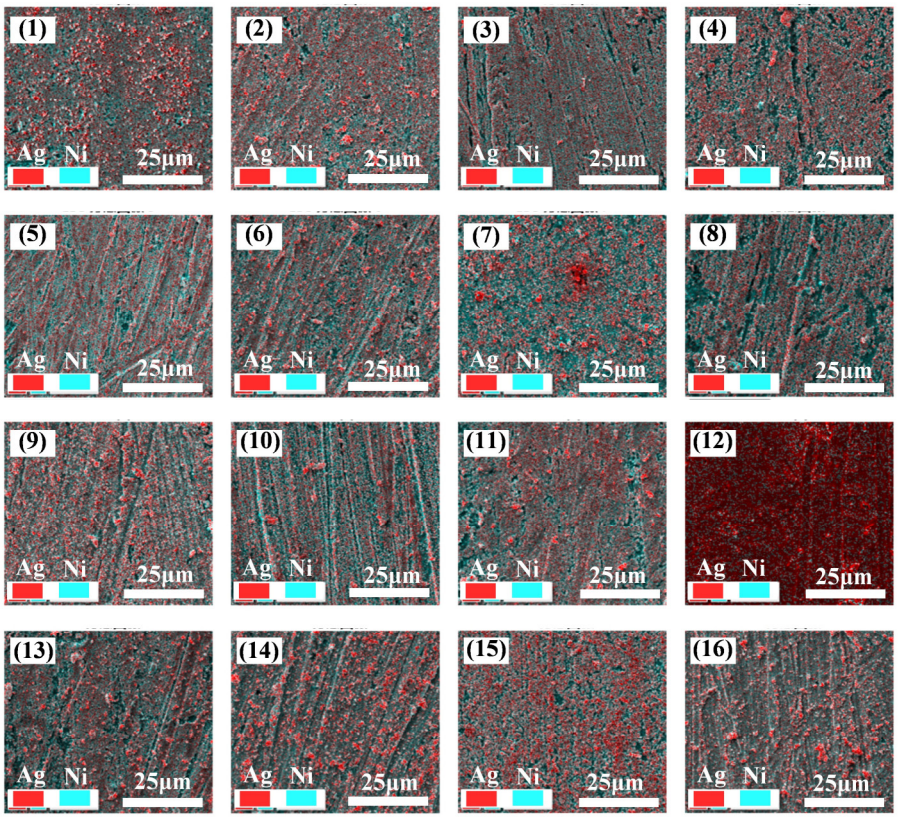


Figure 2. The results of the EDS detection of silver films.

The p-value of this model is 0.013, so the model is significant; and its p-value of lack of fit is 0.0816, so there is no lack of fit factor. The analysis of variance (ANOVA) test shows that X_1 has an extremely significant impact on the regression equation (p_1 = 0.0006). X_2, X_1', and X_3' have a significant impact on the regression equation (p_2 = 0.049, p_1' = 0.033, p_3'= 0.036). According to the magnitude of the coefficients, it can be concluded that the order of influence of these three factors on the silver content on the surface of the film is as follows: plating current > plating time > plating temperature.

Substituting the quadratic term centering formula and coding formula into the above formula, the quadratic regression constraint equation (regression formula) of silver content (n) can be obtained as:

$$n = -3.247 + 6.997I - 0.00364t + 0.125T + 0.00527It - 0.00815IT + 5.918 \times 10^{-5}tT - 13.628I^2 + 3.081t^2 - 0.00133T^2 \quad (4)$$

We used the solver function of Excel software (version 16) to predict the optimal value of the regression Equation (4) under the designed experimental conditions. The results show that X_1 = 0.28, X_2 = 180, and X_3 = 50.5; that is, when I = 0.28 mA, t = 180 s, and T = 50.5 °C, the silver content of the film reaches the maximum value, and the value is 0.73. When X_1 = 0.1, X_2= 60, and X_3 = 60; that is, when I = 0.1 mA, t = 60 s, T = 60 °C, the silver content of the film reaches the minimum value, and the value is 0.06.

2.3. Testing Silver Films with Confocal Microscopy

Confocal microscopy was used to measure the thickness (h), surface roughness (Rc), and surface area to area ratio (a) of the silver film. The thickness of the silver film is measured by removing the prefabricated insulating adhesive on the nickel substrate and measuring the thickness of the silver film in its vicinity, and the film thickness is measured under a confocal microscope lens of 100 times magnification. The surface roughness and surface area to area ratio were measured under a 50× confocal microscope lens, and these data are averages of the five positions measured in the obtained confocal micrographs. The regression analysis in Excel software was used to perform a quadratic orthogonal regression analysis with the thickness, surface roughness, and surface area to area ratio as indicators. The experimental results of the binary quadratic regression orthogonal combination design are shown in Table 1.

Table 1. The results of the quadratic orthogonal regression analysis using surface roughness Rc, surface area to area ratio a, and thickness h as indicators, respectively.

Norm		**Intercept**	X_1	X_2	X_3	X_1X_2	X_1X_3
Rc	Coefficients	0.440941	0.019841	0.022194	0.043314	−0.02212	−0.08117
	p-value	6.12×10^{-8}	0.270713	0.22364	0.038125	0.29879	0.005858
a	Coefficients	1.088061	0.013394	0.023726	0.012756	0.012769	−0.0175
	p-value	2.78×10^{-13}	0.041474	0.003773	0.048981	0.083589	0.029554
h	Coefficients	0.712833	0.115098	0.111106	0.115758	−0.04388	0.052625
	p-value	7.8×10^{-7}	0.029628	0.033738	0.029003	0.397961	0.316997
Norm		X_2X_3	X_1'	X_2'	X_3'	p	p_{lack}
Rc	Coefficients	0.035704	−0.00485	0.019498	0.051897	0.046535	0.060
	p-value	0.116077	0.843104	0.43814	0.069142		
a	Coefficients	0.009191	0.009672	0.015434	0.014686	0.017	0.18
	p-value	0.186328	0.241208	0.083303	0.095764		
h	Coefficients	−0.03029	0.026261	0.043567	0.18625	0.049	0.06
	p-value	0.553013	0.667769	0.482538	0.018618		

From the data in Table 1, it can be seen that the regression model using surface roughness (Rc) as the index is significant (p = 0.046), and there is no lack of fit factor (p_{lack} = 0.06). Moreover, X_3 has a significant impact on the regression equation (p_1= 0.038), and X_1X_3 has an extremely significant impact on the regression equation (p_{13}= 0.0059). There is a certain interaction between the two factors of plating intensity and plating temperature. The influence of the three factors on surface roughness is as follows: plating temperature > plating time > plating current.

The regression model based on the ratio (a) of surface area to area is significant (p = 0.017), and there is no lack of fit factor (p_{lack}= 0.18). The p-value of the coefficient shows that X_1X_3 have a significant impact on the regression equation (p_{13} = 0.03), and X_2 has an extremely significant impact on the regression equation (p_2 = 0.0038). There is a certain interaction between the two factors of plating intensity and plating temperature. The influence of the three factors on the ratio of surface area to area is: plating time > plating current > plating temperature.

The regression model of film thickness h is significant (p = 0.049), and there is no lack of fit factor (p_{lack}= 0.06). The p-values of the fitting results in the Table show that X_1, X_2, X_3, and X_3' have a significant effect on the regression equation ($0.01 < p < 0.05$). The influence of the three factors on film thickness is: plating temperature > plating current > plating time.

The quadratic term-centered formula and coding formula are represented in the regression model in Table 1. After sorting, the coefficients of the quadratic regression constraint equation of the three indicators under natural variables can be obtained, as shown in Table 2.

Table 2. Coefficient table of the three indicator models under natural variables.

	Intercept	*I*	*t*	*T*	*It*	*IT*
Rc	1.359237	8.011119	−0.00539	−0.06546	−0.00608	−0.13393
a	1.602753	0.557335	−0.00316	−0.0199	0.003511	−0.02887
h	7.451364	−3.13415	0.004176	−0.30079	−0.01207	0.086831
	tT	I^2	t^2	T^2	Minimum value	maximum value
Rc	9.86×10^{-5}	−0.82333	8.98×10^{-6}	0.00086	0.389	0.675
a	2.54×10^{-5}	1.592537	7.09×10^{-6}	0.000243	1.037	1.197
h	-8.4×10^{-5}	4.29626	2×10^{-5}	0.003084	0.274	1.359

Use Excel software to plan and solve the regression equation and predict the optimal value under the designed experimental conditions. Within the scope of this electroplating experimental condition, the maximum value of the surface roughness (*Rc*) of the silver film is 0.675 μm, and its minimum value is 0.389 μm. The maximum value of the ratio (*a*) of surface area to area is 1.197, and its minimum value is 1.037. The maximum value of the silver film thickness (*h*) is 1.359 μm, and its minimum value is 0.274 μm.

Through the quadratic orthogonal regression fitting results in Table 2, it is found that the surface roughness, surface area to area ratio, and thickness of silver films are affected by the electroplating current, plating time, and plating temperature. And the effects of the three plating conditions on the surface roughness, surface area to area ratio, and thickness are all positively correlated.

2.4. Analysis of Variance and Interaction Effects of Regression Model Indexed by the Catalytic Decomposition Reaction Rate r of Hydrogen Peroxide

The concentration value of hydrogen peroxide solution before and after catalytic decomposition in the catalytic chip was determined, and the reaction rate (*r*) of hydrogen peroxide solution under the catalytic action of the catalytic bed of the silver film microchannel was calculated by Equation (9). It is possible to compare the changes in the reaction rate of the hydrogen peroxide-catalyzed decomposition of silver films obtained under different plating conditions.

A regression model of the reaction rate (*r*) of hydrogen peroxide reaction solution under the catalytic action of the microchannel catalytic bed of the silver membrane can be obtained. The formula is as follows:

$$R = 65.92 + 0.2747X_1 + 1.2327X_2 - 2.2901X_3 - 1.2788X_1X_2 + 0.7956X_1X_3 + 13.8867X_2X_3 + 6.7469X_1{}' + 1.8492X_2{}' + 2.5577X_3{}' \quad (5)$$

The regression model is significant ($p = 0.015$) and has no lack of fit factors ($p_{lack} = 0.082$). An ANOVA test showed that $X_1{}'$ had a significant effect on the regression equation ($p_1{}'$=0.031) and X_2X_3 had a significant effect on the regression equation ($p_{23} = 0.004$). There is a certain interaction between the two factors of plating time and plating temperature. The influence of the three factors on the decomposition reaction rate (*r*) is as follows: plating temperature > plating time > plating current.

Substituting the quadratic term-centered formula and coding formula into the above formula, the quadratic regression constraint equation of the catalytic decomposition reaction rate (*r*) of hydrogen peroxide under the action of the silver film microchannel catalyst can be obtained as:

$$r = 465.24 - 465.026I - 2.0218t - 9.3574T - 0.3517It + 1.3128IT + 0.0383tT - 1112.727I^2 + 0.000841t^2 + 0.042T^2 \quad (6)$$

We used the planning and solving function of Excel software to predict the optimal value of the regression equation under the designed experimental conditions. The results show that the reaction rate of the catalytic decomposition of hydrogen peroxide under the action of the silver film microchannel catalytic bed reaches a maximum value of 99.629 mol·L^{-1}·s^{-1} and a minimum value of 37.431 mol·L^{-1}·s^{-1}.

When the plating time is 120 s and the plating temperature is 54 °C, the effect of the plating current (*I*) on the reaction rate (*r*) of the catalytic decomposition of hydrogen peroxide reaction solution under the action of the silver thin film microchannel catalytic bed is as shown in Figure 3a. When the plating current (*I*) is in the range of 0.1 mA~0.3 mA, the reaction rate (*r*) of catalytic decomposition first decreases and then increases with the increase in current intensity (*T*). At a plating current of 0.21 mA, the reaction rate (*r*) of catalytic decomposition reaches a minimum.

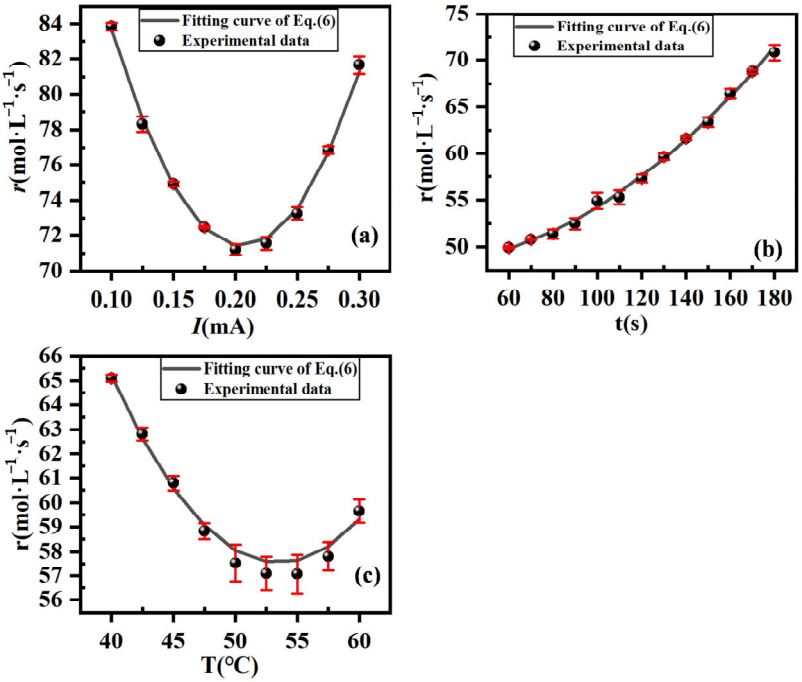


Figure 3. Trend chart of the influence of electroplating conditions on the reaction rate *r* of the decomposition of hydrogen peroxide reaction solution under the action of the microchannel catalytic bed. $t = 120$ s, $T = 54$ °C, I (0.1 mA~0.3 mA) (**a**). $I = 0.2$ mA, $T = 54$ °C, t (60 s~180 s) (**b**). $t = 120$ s, $I = 0.2$ mA°C, T (0 °C~60 °C) (**c**).

When the plating current (*I*) is 0.2 mA and the plating temperature (*T*) is 54 °C, the effect of plating time (*t*) on the reaction rate (*r*) of the catalytic decomposition of hydrogen peroxide reaction solution under the action of the silver thin film microchannel catalytic bed is shown in Figure 3b. When the plating time (*t*) is in the range of 60 s~180 s, the reaction rate (*r*) of catalytic decomposition gradually increases with the increase in plating time.

According to the one-factor theoretical analysis based on the mathematical model, Figure 3c shows the effect of the plating temperature (*T*) on the reaction rate (*r*) of the catalytic decomposition of hydrogen peroxide reaction solution under the action of the silver thin film microchannel catalytic bed when the plating current is 0.2 mA and the plating time is 120 s. When the plating temperature is in the range of 40 °C~60 °C, the reaction rate (*r*) of catalytic decomposition first decreases and then increases with the increase in electroplating temperature (*T*). At the plating temperature of 53.5 °C, the reaction rate (*r*) of catalytic decomposition reaches a minimum.

The experimental results in Figure 3 show that the reaction rate of the catalytic decomposition of hydrogen peroxide under the catalytic action of the microchannel catalytic bed of the silver film will be significantly affected by the plating current, plating time, and plating temperature. And these three plating conditions have a quadratic correlation with the reaction rate of the catalytic decomposition of hydrogen peroxide. This is similar to the fitting curve of regression Equation (6), which proves the significant fitting relationship of regression Equation (6).

2.5. Effect of Silver Film Surface Structure on the Reaction Rate r of Catalytic Decomposition

The reaction rate (r) of the catalytic decomposition of the hydrogen peroxide reaction liquid under the action of the silver film microchannel catalytic bed is used as the index. Surface roughness (Rc), average particle size of silver particles (d), silver content (n), film thickness (h), and surface area to area ratio (a) are used as the natural variables of the model. In addition, the regression analysis was carried out using the reaction rate of catalytic decomposition of hydrogen peroxide as the index, and the model equation of the catalytic decomposition reaction rate (r) was obtained as follows

$$r = -153.382 + 0.254d - 14.686n + 15.044Rc + 179.26a - 10.961h \quad (7)$$

The model is extremely significant (p = 0.009), and there is no lack of fit factor. The p-value analysis of the coefficients shows that d has an extremely significant impact on the regression equation (p = 0.0068), and a has a significant impact on the regression equation (p = 0.046).

According to the above-mentioned mathematical regression model with the reaction rate (r) of catalytic decomposition as an indicator, the influence of factors such as the average particle size (d) of silver particles, ratio (a) of surface area to area, silver content (n), surface roughness (Rc), and thickness (h) on the reaction rate (r) is studied; the results are shown in Figure 4.

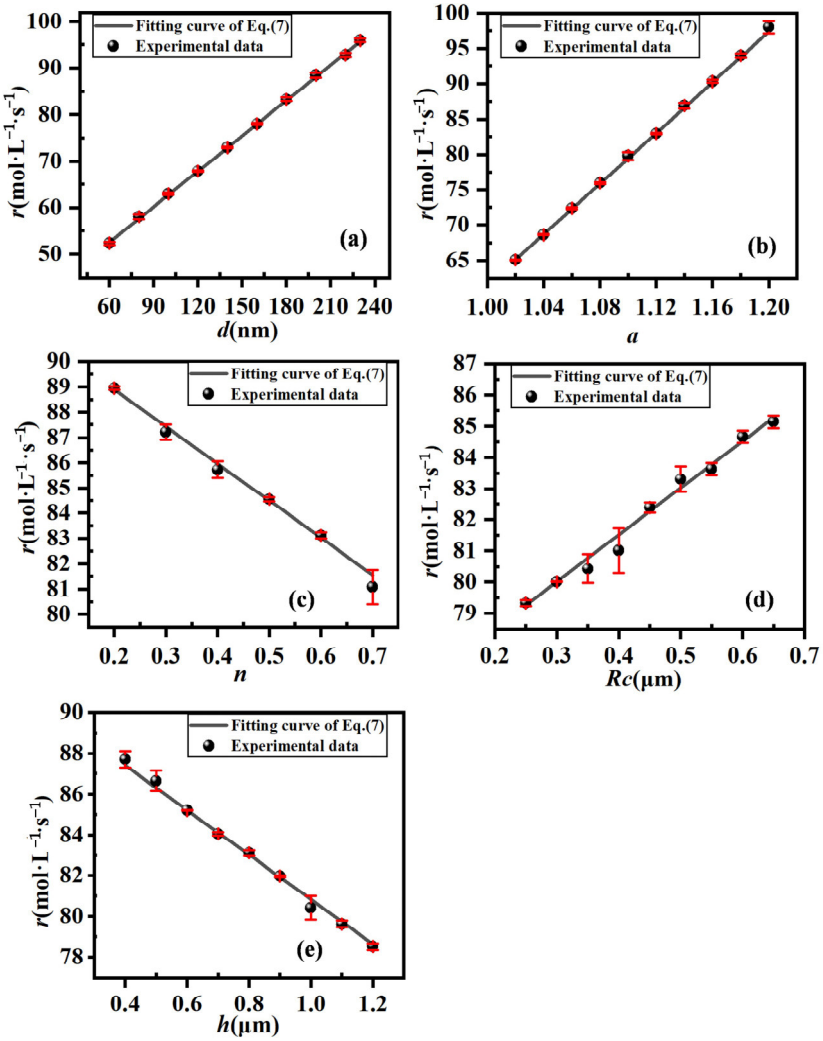


Figure 4. (**a**–**e**) Effect of silver film structure on the reaction rate r of hydrogen peroxide decomposition.

Figure 4a shows the effect of the average particle size of silver particles on the reaction rate (*r*) of hydrogen peroxide decomposition when the silver content (*n*) is 0.6, the surface roughness (*Rc*) is 0.5 μm, the surface area to area ratio (*a*) is 1.12, and the thickness (*h*) is 0.8 μm. When the average particle size (*d*) of silver particles is in the range of 60 to 230 μm, as the average particle size (*d*) of silver particles increases, the catalytic decomposition reaction rate (*r*) will also increase.

Figure 4b shows the effect of the surface area to area ratio (*a*) on the reaction rate (*r*) of hydrogen peroxide decomposition when the average particle size (*d*) of silver particles is 180 nm, the silver content (*n*) is 0.6, the surface roughness (*Rc*) is 0.5 μm, and the thickness (*h*) is 0.8 μm. When the surface area to area ratio (*a*) is in the range of 1.02 to 1.20, as the surface area to area ratio (*a*) increases, the catalytic decomposition reaction rate ®will also increase.

Figure 4c shows the effect of silver content (*n*) on the reaction rate (*r*) of hydrogen peroxide decomposition when the average particle size (*d*) of silver particles is 180 nm, the surface area to area ratio (*a*) is 1.12, the surface roughness (*Rc*) is 0.5μm, and the thickness (*h*) is 0.8 μm. When the silver content (*n*) is in the range of 0.2 to 0.7, as the silver content (*n*) increases, the reaction rate (*r*) of catalytic decomposition will also decrease slightly.

Figure 4d shows the effect of surface roughness (*Rc*) on the reaction rate (*r*) of hydrogen peroxide decomposition when the average particle size (*d*) of silver particles is 180 nm, the surface area to area ratio (*a*) is 1.12, the silver content (*n*) is 0.6, and the thickness (*h*) is 0.8 μm. When the surface roughness (*Rc*) is in the range of 0.25~0.65 μm, as the silver content (*n*) increases, the reaction rate (*r*) of catalytic decomposition will also increase slightly.

Figure 4e shows the effect of thickness (*h*) on the reaction rate (*r*) of hydrogen peroxide decomposition when the average particle size (*d*) of silver particles is 180 nm, the surface area to area ratio (*a*) is 1.12, the silver content *n* is 0.6, and the surface roughness *Rc* is 0.5 μm. When the thickness (*h*) is in the range of 0.4~1.2, as the silver content (*n*) increases, the reaction rate (*r*) of catalytic decomposition decreases slightly.

The results in Figure 4 show that the reaction rate of the catalytic decomposition of hydrogen peroxide under the catalytic action of the microchannel catalytic bed is greatly affected by the ratio of the surface area to area of the silver film (*a*) and the average particle size of the silver particles on the surface of the film (*d*), and the effect of these two factors on the reaction rate is positively correlated. However, silver content (*n*), surface roughness (*Rc*), and thickness (*h*) have little effect on the reaction rate of the catalytic decomposition of hydrogen peroxide. The results of this experiment are also in good agreement with the fitting results of regression Equation (7).

2.6. Confirmatory Experiments at Optimal Process Points

According to the regression model of the surface area ratio (*a*), surface roughness (*Rc*), thickness (*h*), catalytic decomposition reaction rate(*r*), silver content, and average particle size (*d*) of silver particles, the results are shown in Table 3. We used Excel software to plan and solve the four regression models to obtain the minimum values of their respective equations. We then used the following formula:

$$F = \sum(Q_{\max} - Q)/(Q_{\max} - Q_{\min}) + \sum(P - P_{\min})/(P_{\max} - P_{\min}) \quad (8)$$

where Q is the average particle size d of silver particles, the ratio (a) of surface area to area, thickness (d), and silver content (n); and P is the surface roughness (Rc) of the silver film.

We used Excel software to plan and solve the equation and find the maximum value of equation F. The silver film prepared here has the surface area to area ratio (a), thickness (h), catalytic decomposition reaction efficiency (r), and silver content (n) being as large as possible, while the surface roughness (Rc) and the average particle size (d) of silver particles is as small as possible for optimal electroplating conditions. After planning and solving, plating current I = 0.3 mA, plating time t = 180 s, and plating temperature T = 60 °C are the optimal electroplating experimental conditions. At this time, the surface area to area ratio *a*

of the silver film obtained by electroplating is 1.197, the surface roughness *Rc* is 0.503 μm, the thickness *h* is 1.359 μm, and the catalytic decomposition reaction rate *r* of hydrogen peroxide by the silver film microchannel catalyst is 97.608 mol·L^{-1}·s^{-1}. The silver content *n* is 0.603, and the average particle size *d* of silver particles is 196.692 nm.

Table 3. Data sheet for the optimization of plating conditions.

	Intercept	***I***	***t***	***T***	***It***	***IT***
Rc	1.359	8.011	−0.00539	−0.0655	−0.00608	−0.134
r	465.237	−465.026	−2.0218	−9.357	−0.352	1.313
h	7.451	−3.134	0.00418	−0.301	−0.0121	0.0868
a	1.603	0.557	−0.00316	−0.0120	0.00351	−0.0289
d	947.950	−2184.245	−4.772	−10.616	1.031	26.400
n	−3.247	6.997	−0.00365	0.126	0.00527	−0.00815
	tT	I^2	t^2	T^2	Minimum value	maximum value
Rc	9.857×10^{-5}	−0.823	8.979×10^{-6}	0.000860	0.389	0.675
r	0.0383	1112.727	0.000841	0.0420	37.431	99.629
h	-8.362×10^{-5}	4.296	2.001×10^{-5}	0.00308	0.274	1.359
a	2.537×10^{-5}	1.593	7.087×10^{-6}	0.000243	1.037	1.197
d	0.109	1920.403	−0.00453	−0.0930	38.338	196.692
n	5.918×10^{-5}	−13.628	3.081×10^{-6}	−0.00133	0.137	0.732

Validation experiments showed that the surface area to area ratio (1.195 ± 0.002), surface roughness (0.514 ± 0.003 μm), film thickness (1.346 ± 0.005 μm), catalytic decomposition rate of hydrogen peroxide by the silver film microchannel catalysts (98.02 ± 1.50 mol·L^{-1}·s^{-1}), silver content(0.618), and average particle size of silver particles (192 nm) were in general agreement with the predictions of the regression model. The optimized silver thin films are consistent with the results of the silver thin films prepared by the ANOVA test and with the interaction effects of the regression model in Section 2.5 using only the catalytic decomposition rate *r* of hydrogen peroxide when using the silver microchannel catalyst as an indicator. It is proven that the microchannel catalytic decomposition efficiency of silver thin films obtained by this method is the highest, and the surface roughness of silver thin films prepared at this time is also smaller; the ratio of the surface area to the area and the thickness are also relatively large. This provides a good optimization scheme for the preparation of microchannel catalysts for the hydrogen peroxide decomposition reaction in microfluidic microreactors.

3. Experiment

3.1. Experimental Reagents and Equipment

Silver nitrate (Xilong scientific (Shantou, China), AR), butyldiimide (ShanDong Guohua, (Jinan, China), AR), and potassium hydroxide (Weilian chem (Jiaozuo, China), AR) were used to configure the silver plating solution. Nickel sheet (purity 99.99%, 2 mm × 6 mm × 0.5 mm) was used as the electroplating cathode substrate, and platinum sheet (10 mm × 10 mm × 0.2 mm) was used as the electroplating anode plate. Alcohol and acetone were used for cleaning the nickel sheet and quartz glass sheet. A standard solution of cerium sulfate with a concentration of 0.1 mol·L^{-1} was used to determine the concentration of the hydrogen peroxide solution [43]. We used 30% hydrogen peroxide solution (HUSHI (Shanghai, China), AR) and deionized water to prepare a hydrogen peroxide reaction solution with a volume fraction of 5%.

A CS electrochemical workstation (Corrtest Instrument (Wuhan, China), CS310M EIS Potentiostat/Galvanostat) was used to electroplate silver on pure nickel sheets. A peristaltic pump (LEADFLUID (Baoding, China), BT 600F), heating table, and plastic thin tube were used to analyze the decomposition performance of the silver catalyst microchannel. Quartz glass and photosensitive adhesive were used to prepare microchannel chips. Laser confocal microscopy (OLYMPUS (Tokyo, Japan), OLS3100) was used to obtain the surface structure of electroplated silver films. Ultraviolet-Vis spectroscopy (Beijing Avantes Technology Co., Ltd. (Beijing, China), AvaSpec ULS2048L-USB2), a full-band light

source (Beijing Avantes Technology Co., Ltd. (Beijing, China), AVALIGHT-HAL-MINT s/n: LS-1608038), and microcell cells were used to indirectly determine the concentration of hydrogen peroxide solutions.

3.2. Silver Microchannel Catalytic Bed Prepared by Cyanide-Free Plating Method

In order to obtain silver films with different surface morphology structures, a cyanide-free plating technique was used to conduct constant-current silver plating experiments using butanediimide as a ligand, which was co-dissolved with silver nitrate in distilled water as the plating solution for silver plating; the prepared silver film samples were compared. The other experimental parameters for the preparation of silver films using cyanide-free plating were the same: the concentration of succinimide in the plating solution was 16 g/L, the concentration of silver nitrate was 4 g/L, and the pH value was above 8.5; the cathode was a nickel sheet with the dimensions of 2 mm × 6 mm × 0.5 mm that only existed on the upper surface; the anode was a platinum sheet with the dimensions of 10 mm × 10 mm × 0.2 mm; and the reference electrode was a Hg/HgO electrode. The electroplating experimental setup diagram and electrode reaction equation are shown in Figure 5. The experiment was carried out using a quadratic regression orthogonal test program.

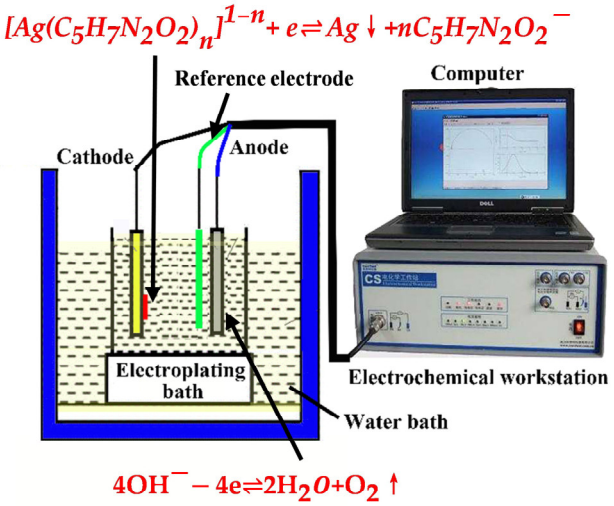


Figure 5. Diagram of the electroplating experimental setup and electrode reaction equation.

In this study, we analyzed the relationship between three factors, namely current intensity I (0.1 mA to 0.3 mA), electroplating time t (60 s to 180 s), and water bath temperature T (40 °C to 60 °C), on the film thickness, surface roughness, and surface area to area ratio based on a quadratic regression orthogonal test. Because the number of factors m = 3, if the number of zero level tests m_0 = 2 is taken, r = 1.287 is obtained according to the formula of the asterisk arm length (r).

According to the factor $I(X_1)$, the upper limit $X_1^{1.287}$ is 0.3 mA and the lower line ${X_1}^{-1.287}$ is 0.1 mA; thus, the zero level X_1^0 is 0.2 mA, the variation spacing Δj is 0.078 mA, the upper level X_1^1 is 0.278 mA, and the lower level ${X_1}^{-1}$ is 0.122 mA. Similarly, the coding of the factors $t(X_2)$ and $T(X_3)$ can be calculated as shown in Table 4.

Due to the number of factors m = 3, orthogonal table $L8(2^7)$ was chosen for transformation, and the number of two-level tests was $m_c = 2^3 = 8$. The other factors were designed according to the values obtained from the previous calculations, and 16 groups of experimental modules were obtained. According to the requirements of the binary quadratic regression orthogonal combination design, the quadratic terms ${X_1}^2$, ${X_2}^2$, and ${X_3}^2$ were centered to obtain ${X_1}'$, ${X_2}'$, and ${X_3}'$, respectively.

Table 4. Table of factors and levels.

Levels Code X_j	Natural Variables		
	I (mA)	t (s)	T (°C)
1.287	0.300	180.000	60.000
1	0.278	166.620	57.770
0	0.200	120.000	50.000
−1	0.122	73.380	42.230
−1.287	0.100	60.000	40.000
△j	0.078	46.620	7.770

3.3. Catalytic Performance of Silver Thin Film Microchannel Catalytic Beds

A microchannel catalytic bed was formed by using an electroplated silver film as the bottom material of the catalytic bed, paired with a solid tape. The microchannel catalytic bed was sealed into a homemade microcatalytic chip, and the catalytic decomposition reaction rate of this microchannel catalytic bed on the hydrogen peroxide reaction solution was measured under microfluidic conditions and compared with the catalytic decomposition reaction rate of the silver film on the nickel sheet obtained by the quadratic regression orthogonal test.

The silver film microchannel catalytic bed was firstly prepared using the same preparation process as shown in Figure 6. The silver film microchannel catalytic bed consists of three layers, namely a nickel sheet with a bottom dimension of 2 mm × 6 mm × 1.4 mm, a silver film with a thickness of a few micrometers in the middle layer, and two plastic tapes with a dimension of 0.75 mm × 6 mm × 0.1 mm on the top layer to form the walls of the flow channel. The formed catalytic bed microfluidic channel was rinsed and dried to ultimately obtain a clean and dry silver microchannel catalytic bed with the dimensions of 0.5 mm × 6 mm × 0.1 mm.

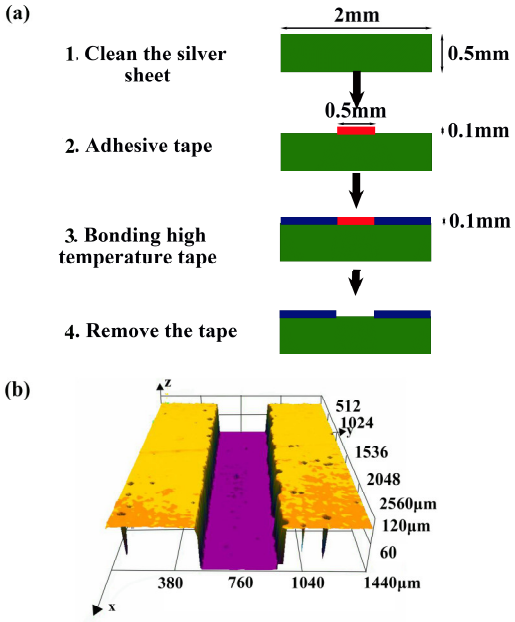


Figure 6. Flowchart of the preparation of the silver film microchannel catalytic bed (**a**) and three-dimensional confocal microscope view of the catalytic bed (**b**).

Figure 7a shows the flow channel structure of the catalytic chip. Figure 7b shows the structure of the catalytic bed and the equation for the catalytic decomposition reaction of hydrogen peroxide that occurs on the wall. The flow of the catalytic reaction chip prepared by the MEMS process is shown in Figure 7c. The catalytic reaction chip consisted of a quartz glass substrate engraved with microfluidic channels with a thickness of 1.5 mm and a quartz glass cover plate with a thickness of 1 mm, as well as a silver film catalytic bed. Among them, the substrate and cover plate were sealed by photosensitive adhesive,

and the non-fluidized part of the silver film microchannel catalytic bed was filled by high-temperature adhesive so as to form a microcatalytic chip with an external dimension of 22 mm × 32 mm × 2.5 mm.

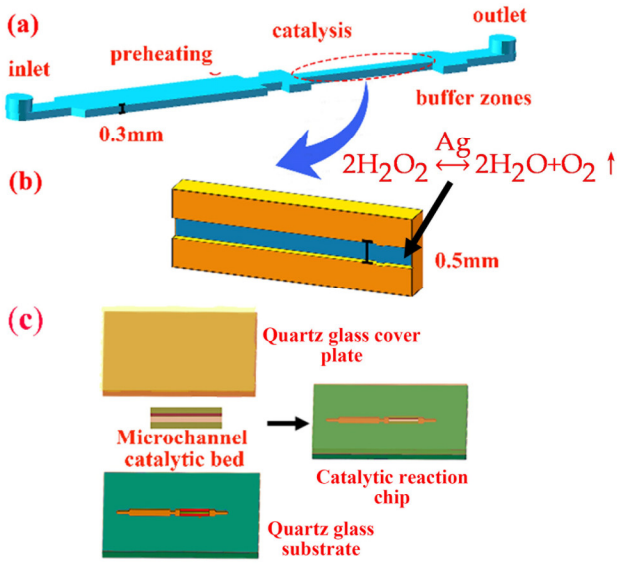


Figure 7. Structural diagram of the flow channel of the catalytic reaction chip (**a**), structural diagram of a thin film microchannel catalytic bed and reaction formula for the hydrogen peroxide-catalyzed decomposition (**b**), and flow chart of the preparation of the catalytic reaction chip (**c**).

The structure of the device for measuring the rate of the catalytic decomposition reaction of hydrogen peroxide reaction solution by the microchannel catalytic bed is shown in Figure 8. The device consists of a peristaltic pump, a preheating spiral pipe, a catalytic reaction chip, a cooling spiral pipe, and other parts. The test process used the same flow rate and same concentration of hydrogen peroxide reaction liquid injected into the catalytic reaction chip, and the catalytic decomposition reaction rate was calculated by monitoring the concentration value of the reaction liquid at the entrance and exit.

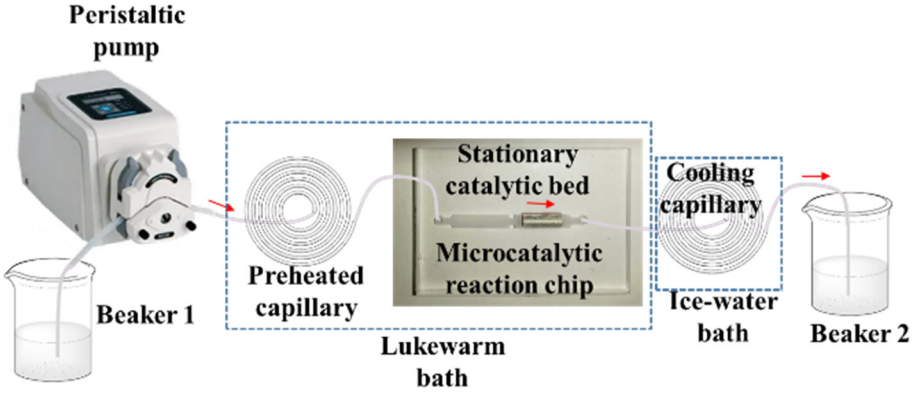


Figure 8. Experimental setup for the catalytic decomposition of hydrogen peroxide reaction solution under the action of silver thin film microchannel catalytic beds.

Among them, the volume fraction of the hydrogen peroxide reaction solution was 5%, the catalytic reaction chip was heated on a heating plate at 40 °C, and the flow rate of hydrogen peroxide reaction solution was q = 10 mL·min^{-1}. The molar concentration of hydrogen peroxide reaction solution before injection was measured by a portable spectrometer as c_0, and the concentration of the hydrogen peroxide reaction solution at the outlet was c_t. The total volume of the microchannel of the catalytic bed is V_0 = 0.0003 mL, and the residence

time of the hydrogen peroxide reaction solution in the silver film microchannel catalytic bed is $t = V_0/q = 0.00072$ s. Therefore, the catalytic decomposition reaction rate r is

$$r = (c_0 - c_t)/t \quad (9)$$

The concentration of the hydrogen peroxide reaction was measured indirectly by a portable ultraviolet visible optical spectrometer; the test device is shown in Figure 9a. The physical image of the microcell is shown in Figure 9b, and the optical path length of the spectral detection is 10 mm. The absorption value of hydrogen peroxide solution after the reaction of hydroxide solution was determined by indirect measurement, and the concentration was calculated. Equation (9) was applied to calculate the reaction rate of the catalytic decomposition of hydrogen peroxide in a catalytic reaction chip in a microchannel catalytic bed of a silver film.

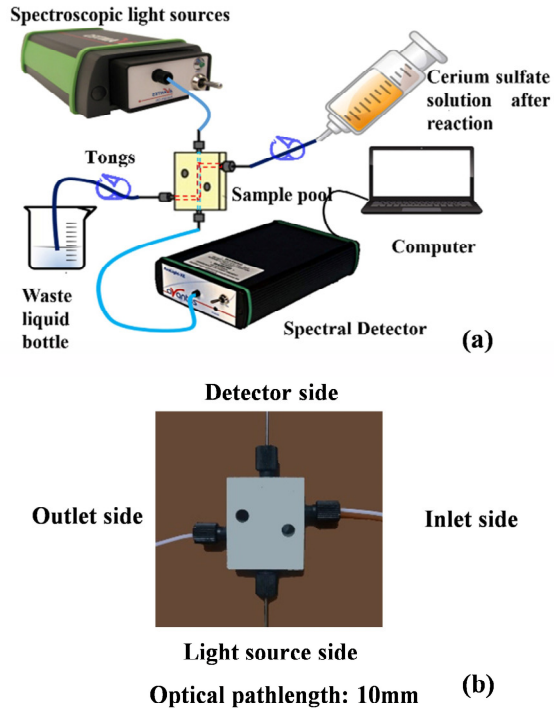


Figure 9. Installation diagram for the spectroscopic testing of hydrogen peroxide concentration (**a**). Physical image of the microsample cell (**b**).

4. Conclusions

This article designed and prepared a microfluidic reaction chip containing a microchannel catalytic bed and applied it to detect the reaction rate of the catalytic decomposition of hydrogen peroxide reaction solution under the action of a microchannel catalytic bed with a silver film as the bottom material. At the same time, a silver film with a thickness of several microns was prepared on nickel sheets by galvanostatic-free cyanide-free plating, and its surface structure and catalytic reaction performance were analyzed using quadratic orthogonal regression.

In the regression model using the reaction rate of the catalytic decomposition of the hydrogen peroxide reaction by the microchannel catalytic bed of silver thin film as the index, the secondary term of the current intensity has a significant effect on the reaction rate of hydrogen peroxide decomposition, the product of the plating time and plating temperature has an extremely significant effect on the reaction rate of hydrogen peroxide decomposition, and there is a certain interaction between the two factors of plating strength and plating temperature. The average particle size and surface area to area ratio of silver particles on the surface of silver films have a significant positive correlation with the reaction rate of

the catalytic decomposition of hydrogen peroxide reaction in the microchannel catalytic bed, but the surface roughness, silver content, and film thickness have little effect on the reaction rate of catalytic decomposition.

Through the multi-objective optimization design and experiments, it can be seen that when the current intensity is 0.3 mA, the plating time is 180 s, and the plating temperature is 60 °C, the prepared silver thin film is the optimal solution. At this time, the ratio of the surface area to area of the silver film is 1.195 ± 0.002, the thickness is 1.346 ± 0.005 μm, and the surface roughness is 0.514 ± 0.003 μm. The reaction rate of the hydrogen peroxide reaction solution catalyzed by the microchannel catalytic bed of silver thin film was 98.02 ± 1.50 $mol \cdot L^{-1} \cdot s^{-1}$. The EDS measured a silver content of 0.618. SEM observation showed that the average particle size of silver particles on the surface of the film was 192 nm.

The silver film used in this paper was composed of pure silver, and there is a lack of research on the effects of composite thin film catalysts with other auxiliary materials and more complex microchannel catalytic beds on the reaction rate of the catalytic decomposition of hydrogen peroxide reaction solution; therefore, it is necessary to pay attention to the influence of these factors in subsequent studies.

Author Contributions: Conceptualization, writing—original draft preparation, Y.Y. (Yang Yong) and Y.Y. (Yinghua Ye); supervision, review, and editing, R.S. All authors have read and agreed to the published version of the manuscript.

Funding: This research received no external funding.

Data Availability Statement: Data are contained within the article.

Acknowledgments: Yang Yong thanked his colleagues from the Micro-Nano Energetic Devices Key Laboratory of MIIT Institute of Space Propulsion and Information Technology for their support in the preparation of this manuscript. All authors would like to thank their departments for their support in preparing this manuscript.

Conflicts of Interest: The authors declare no conflict of interest.

Nomenclature

X_1	Regression variable 1
X_2	Regression variable 2
X_3	Regression variable 3
X_1'	The normalized value of X_1 squared
X_2'	The normalized value of X_2 squared
X_3'	The normalized value of X_3 squared
c_0	Initial concentration (mol/L)
c_t	Concentration after catalytic decomposition reaction (mol/L)
t_0	The residence time of the reaction solution in the microchannel catalytic bed (s)
t	Plating time (s)
T	Plating temperature (°C)
I	Plating current (mA)
q	The flow rate of the reaction solution (mL/min)
V_0	The volume of the flow channel of the microchannel catalytic bed (mm^3)
a	The ratio of surface area to area, where surface area refers to the actual area of the surface of the silver film and area refers to the area of the surface of the film projected on a plane on a nickel substrate.
n	The content of silver
h	Film thickness (μm)
Rc	Surface roughness (μm)
d	The average particle size of silver particles (nm)
r	The reaction rate of catalytic decomposition ($mol \cdot L^{-1} \cdot s^{-1}$)
ANOVA	Analysis of variance
CS work station	Electrochemical workstations
MEMS	Microelectromechanical systems

References

1. Gauer, M.; Telitschkin, D.; Gotzig, U.; Batonneau, Y.; Johansson, H.; Ivanov, M.; Palmer, P.; Wiegerink, R. First Results of PRECISE—Development of a MEMS-Based Monopropellant Micro Chemical Propulsion System. *Acta Astronaut.* **2014**, *93*, 77–83. [CrossRef]
2. Huh, J.; Kwon, S. Design, fabrication and thrust measurement of a micro liquid monopropellant thruster. *J. Micromech. Microeng.* **2014**, *24*, 104001. [CrossRef]
3. Hitt, D.L.; Zakrzwski, C.M.; Thomas, M.A. MEMS-based satellite micropropulsion via catalyzed hydrogen peroxide decomposition. *Smart Mater. Struct.* **2001**, *10*, 1163. [CrossRef]
4. Luo, N.; Miley, G.H.; Gimlin, R.J.; Burton, R.L.; Rusek, J.; Holcomb, F. Hydrogen-Peroxide-Based Fuel Cells for Space Power Systems. *J. Propuls. Power* **2008**, *24*, 583–589. [CrossRef]
5. Kuan, C.K.; Chen, G.B.; Chao, Y.C. Development and Ground Tests of a 100-Millinewton Hydrogen Peroxide Monopropellant Microthruster. *J. Propuls. Power* **2015**, *23*, 1313–1320. [CrossRef]
6. Palmer, M.; Roberts, G.; Musker, A. Design, Build and Test of a 20 N Hydrogen Peroxide Monopropellant Thruster. In Proceedings of the 47th AIAA/ASME/SAE/ASEE Joint Propulsion Conference & Exhibit, San Diego, CA, USA, 31 July–3 August 2011.
7. Krejci, D.; Woschnak, A.; Schiebl, M.; Scharlemann, C.; Ponweiser, K.; Brahmi, R.; Batonneau, Y.; Kappenstein, C. Assessment of catalysts for hydrogen-peroxide-based thrusters in a flow reactor. *J. Propuls. Power* **2013**, *29*, 321–330. [CrossRef]
8. Okninski, A.; Bartkowiak, B.; Sobczak, K.; Kublik, D.; Surmacz, P.; Rarata, G.; Marciniak, B.; Wolanski, P. Design and testing of a Small Green Bipropellant Rocket Engine Using Hydrogen Peroxide as Oxidizer. In Proceedings of the 50th AIAA/ASME/SAE/ASEE Joint Propulsion Conference, Cleveland, OH, USA, 28–30 July 2014. [CrossRef]
9. Kang, H.; Jang, D.; Kwon, S. Demonstration of 500 N scale bipropellant thruster using non-toxic hypergolic fuel and hydrogen peroxide. *Aerosp. Sci. Technol.* **2016**, *49*, 209–214. [CrossRef]
10. Krejci, D.; Woschnak, A.; Scharlemann, C.; Ponweiser, K. Performance Assessment of 1 N Bipropellant Thruster Using Green Propellants H2O2/Kerosene. *J. Propuls. Power* **2013**, *29*, 285–289. [CrossRef]
11. Scharlemann, C. Green Advanced Space Propulsion—A project status. In Proceedings of the AIAA/ASME/SAE/ASEE Joint Propulsion Conference & Exhibit, San Jose, CA, USA, 15–17 July 2013. [CrossRef]
12. Latifoglu, A.; Kilic, A. An investigation of catalytic decomposition of hydrogen peroxide by iron oxide in water. *Fresenius Environ. Bull.* **2002**, *11*, 894–898.
13. Amri, R.; Gibbon, D.; Rezoug, T. The design, development and test of one newton hydrogen peroxide monopropellant thruster. *Aerosp. Sci. Technol.* **2013**, *25*, 266–272. [CrossRef]
14. Krejci, D.; Woschnak, A.; Scharlemann, C.; Ponweiser, K. Structural impact of honeycomb catalysts on hydrogen peroxide decomposition for micro propulsion. *Chem. Eng. Res. Des.* **2012**, *90*, 2302–2315. [CrossRef]
15. Kang, S. Catalyst bed behavior of hydrogen peroxide/kerosene bipropellant thruster in monopropellant and bipropellant modes with cavitating venturi valve. *Acta Astronaut.* **2023**, *205*, 47–56. [CrossRef]
16. Jeong, J.; Bhosale, V.K.; Kwon, S. Ultrafast igniting, low toxicity hypergolic hybrid solid fuels and hydrogen peroxide oxidizer. *Fuel* **2021**, *286*, 119307. [CrossRef]
17. He, W.; Zhou, Y.T.; Wamer, W.G.; Hu, X.; Wu, X.; Zheng, Z.; Boudreau, M.D.; Yin, J.J. Intrinsic catalytic activity of Au nanoparticles with respect to hydrogen peroxide decomposition and superoxide scavenging. *Biomaterials* **2013**, *34*, 765–773. [CrossRef]
18. An, S.; Kwon, S. Scaling and Evaluation of Pt/Al2O3 Catalytic Reactor for Hydrogen Peroxide Monopropellant Thruster. *J. Propuls. Power* **2015**, *25*, 1041–1045. [CrossRef]
19. Wei, P.; Sun, D.; Niu, Y.; Lu, X.; Zhai, H. Enzyme-free electrochemical sensor for the determination of hydrogen peroxide secreted from MCF-7 breast cancer cells using calcined indium metal-organic frameworks as efficient catalysts. *Electrochim. Acta* **2020**, *359*, 136962. [CrossRef]
20. Aguinaco, A.; Pocostales, J.P.; García-Araya, J.F.; Beltran, F.J. Decomposition of hydrogen peroxide in the presence of activated carbons with different characteristics. *J. Chem. Technol. Biotechnol.* **2011**, *86*, 595–600. [CrossRef]
21. Liu, Z.; Shen, Q.; Zhou, C.; Fang, L.; Yang, M.; Xia, T. Kinetic and Mechanistic Study on Catalytic Decomposition of Hydrogen Peroxide on Carbon-Nanodots/Graphitic Carbon Nitride Composite. *Catalysts* **2018**, *8*, 445. [CrossRef]
22. Pirault-Roy, L.; Kappenstein, C.; Guerin, M.; Eloirdi, R.; Pillet, N. Hydrogen Peroxide Decomposition on Various Supported Catalysts Effect of Stabilizers. *J. Propuls. Power* **2002**, *18*, 1235–1241. [CrossRef]
23. Russo, V.; Protasova, L.; Turco, R. Hydrogen Peroxide Decomposition on Manganese Oxide Supported Catalyst: From Batch Reactor to Continuous Microreactor. *Ind. Eng. Chem. Res.* **2013**, *52*, 7668–7676. [CrossRef]
24. Tamami, B.; Ghasemi, S. Catalytic activity of Schiff-base transition metal complexes supported on crosslinked polyacrylamides for hydrogen peroxide decomposition. *J. Organomet. Chem.* **2015**, *794*, 311–317. [CrossRef]
25. Hernandez, K.; Berenguer-Murcia, A.; Rodrigues, R.C.; Fernandez-Lafuente, R. Hydrogen Peroxide in Biocatalysis. A Dangerous Liaison. *Curr. Org. Chem.* **2012**, *16*, 2652–2672. [CrossRef]
26. Sokač Cvetnić, T.; Šalić, A.; Benković, M.; Jurina, T.; Valinger, D.; Gajdoš Kljusurić, J.; Zelić, B.; Jurinjak Tušek, A. A Systematic Review of Enzymatic Kinetics in Microreactors. *Catalysts* **2023**, *13*, 708. [CrossRef]
27. Yang, G.; Park, D.; Kim, C.T.; Kwon, S. Hydrogen Peroxide-Based Gas Generator Design and Performance Testing as an Aircraft Emergency Power Unit. *J. Eng. Gas Turbines Power Trans. ASME* **2010**, *132*, 114504. [CrossRef]

28. Tseng, Y.-W.; Hung, F.-Y.; Lui, T.-S. Thermoelectric Mechanism and Interface Characteristics of Cyanide-Free Nanogold-Coated Silver Wire. *J. Electron. Mater.* **2016**, *45*, 624–630. [CrossRef]
29. Liu, A.; Ren, X.; Yang, Q.; Chen, Y.; Guo, J.; Li, Y.; Gao, L.; An, M. Theoretical and experimental studies of the influence of microstructure on anti-tarnish ability of cyanide-free silver deposit. *Ionics* **2019**, *25*, 849–857. [CrossRef]
30. Furko, M.; Lakatos-Varsányi, M.; Balázsi, C. Complex electrochemical studies on silver-coated metallic implants for orthopaedic application. *J. Solid State Electrochem.* **2016**, *20*, 263–271. [CrossRef]
31. Li, Q.; Qian, H.; Fu, X.; Sun, H.; Sun, J. Characterization and electrochemical analysis of silver electrodeposition in ChCl–urea deep eutectic solvents. *Bull. Mater. Sci.* **2021**, *44*, 14. [CrossRef]
32. Coyle, J.P.; Gordon, P.G.; Wells, A.P.; Mandia, D.J.; Sirianni, E.R.; Yap, G.P.; Barry, S.T. Thermally Robust Gold and Silver Iminopyrrolidinates for Chemical Vapor Deposition of Metal Films. *Chem. Mater.* **2013**, *25*, 4566–4573. [CrossRef]
33. Wu, Y.; Hang, T.; Wang, N.; Yu, Z.; Li, M. Highly durable non-sticky silver film with a microball-nanosheet hierarchical structure prepared by chemical deposition. *Chem. Commun.* **2013**, *49*, 10391–10393. [CrossRef]
34. Das, S.; Mishra, A.; Ghangrekar, M.M. Production of Hydrogen Peroxide Using Various Metal-Based Catalysts in Electrochemical and Bioelectrochemical Systems: Mini Review. *Am. Soc. Civ. Eng.* **2020**, *24*, 06020001. [CrossRef]
35. Basova, E.Y.; Foret, F. Droplet microfluidics in (bio)chemical analysis. *Anal. Anal. J. R. Soc. Chem. A Mon. Int. Publ. Deal. All Branches Anal. Chem.* **2015**, *140*, 22–38. [CrossRef] [PubMed]
36. Patel, K.D.; Bartsch, M.S.; McCrink, M.H.; Olsen, J.S.; Mosier, B.P.; Crocker, R.W. Electrokinetic pumping of liquid propellants for small satellite microthruster applications. *Sens. Actuators B Chem.* **2008**, *132*, 461–470. [CrossRef]
37. Jamal, F.; Jean-Sébastien, G.; Maël, P.; Edmond, P.; Christian, R. Gold nanoparticle synthesis in microfluidic systems and immobilisation in microreactors designed for the catalysis of fine organic reactions. *Microsyst. Technol.* **2012**, *18*, 151–158. [CrossRef]
38. Fan, J.; Lu, J.; Sha, Z.; Zuo, W.; Fei, X.; Zhu, M. Conformally anchoring nanocatalyst onto quartz fibers enables versatile microreactor platforms for continuous-flow catalysis. *Sci. China Chem.* **2021**, *64*, 1596–1604. [CrossRef]
39. Mohammad, N.; Bepari, S.; Aravamudhan, S.; Kuila, D. Kinetics of Fischer–Tropsch Synthesis in a 3-D Printed Stainless Steel Microreactor Using Different Mesoporous Silica Supported Co-Ru Catalysts. *Catalysts* **2019**, *9*, 872. [CrossRef]
40. Ricciardi, R.; Huskens, J.; Verboom, W. Heterogeneous Acid Catalysis Using a Perfluorosulfonic Acid Monolayer-Functionalized Microreactor. *J. Flow Chem.* **2013**, *3*, 127–131. [CrossRef]
41. Xu, B.-B.; Zhang, Y.-L.; Wei, S.; Ding, H.; Sun, H.-B. On-Chip Catalytic Microreactors for Modern Catalysis Research. *ChemCatChem* **2013**, *5*, 2091–2099. [CrossRef]
42. Zhang, L.; Liu, Z.; Liu, L.-Y.; Ju, X.-J.; Wang, W.; Xie, R.; Chu, L.-Y. Novel Smart Microreactors Equipped with Responsive Catalytic Nanoparticles on Microchannels. *ACS Appl. Mater. Interfaces* **2017**, *9*, 33137–33148. [CrossRef]
43. Zhang, Q.; Fu, S.Y.; Li, H.L.; Zhan, H.Y. A rapid method for the determination of hydrogen peroxide concentration. *Spectrosc. Spectr. Anal.* **2014**, *34*, 4.

Disclaimer/Publisher's Note: The statements, opinions and data contained in all publications are solely those of the individual author(s) and contributor(s) and not of MDPI and/or the editor(s). MDPI and/or the editor(s) disclaim responsibility for any injury to people or property resulting from any ideas, methods, instructions or products referred to in the content.